CSIRO OCEANS AND ATMOSPHERE
www.csiro.au

The search for MH370 and ocean surface drift – Part III

David Griffin and Peter Oke
report number EP174155
26 June 2017

Prepared for the Australian Transport Safety Bureau

Citation

Griffin, DA and Oke, PR (2017). The search for MH370 and ocean surface drift – Part III. CSIRO Oceans and Atmosphere, Australia. Report number EP174155. June 2017.

Foreword

This work is dedicated to the 239 people aboard flight MH370.

Contents

Acknowledgments

This work would not have been possible without several data sets; we thank 1) the space agencies NASA, CNES, ESA and ISRO and partner agencies NOAA and EuMetSat for satellite altimetry and radiometer data 2) the Global Drifter Programme of NOAA, which donated 10 SVP drifters to the project as well as providing access to the entire archive of past trajectories of Indian Ocean drifters, and 3) ECMWF, NOAA and BoM for wind and wave data. We thank Australia's Integrated Marine Observing System (IMOS) for supporting the processing and analysis of the satellite data. IMOS is an initiative of the Australian Government through its National Collaborative Research Infrastructure Strategy. The ocean modelling system used for this (and preceding reports) was developed as CSIRO's contribution to the CSIRO Bureau of Meteorology- Royal Australian Navy Bluelink project.

Executive summary

Several high-resolution surveillance satellites were tasked to obtain images of the ocean in the vicinity of the 7th arc while the surface search for missing flight MH370 was underway in March 2014. Many objects of interest were seen in several of these images from a wide range of locations at the time, but none led to any successful recoveries. Four of these images, taken just west of the 7th arc in the vicinity of the new search area proposed by ATSB in 2016, have recently been carefully re-examined (Minchin et al. 2017). Three of these images (referred to as PHR4, PHR3 and PHR1) contained 9, 2 and 1 objects, respectively, that were classified as "probably man-made" as well as 28 "possibly man-made" objects. The dimensions of these objects are comparable with some of the debris items that have washed up on African beaches and their location near the 7th arc makes them impossible to ignore. But there is no evidence to confirm that any of these objects (let alone all) are pieces of 9M-MRO (the aircraft flying as MH370).

To completely reject the possibility that any of these objects are pieces of 9M-MRO is difficult to defend. Consequently, we have addressed the obvious question raised by this new piece of uncertain, but plausibly-relevant evidence:

If at least some objects in the images are pieces of 9M-MRO, from where did they drift in the weeks between the disappearance of the aircraft and image capture?

This question is, perhaps surprisingly, potentially more difficult to answer than the ones we addressed in the two reports preceding this one. This is because it requires a very detailed knowledge of the surface currents out in the middle of the ocean where almost no *in-situ* observations have ever been made. However, thanks to the combined data sets from several types of Earth-observation satellites, coupled with the computational power of Australia's most powerful super-computer and more than a decade of Government investment in operational ocean modelling, we think we have succeeded.

Taking drift model uncertainty into account, we have found that the objects identified in most of the images can be associated with a single location within the previously-identified region suggested by other lines of evidence. Furthermore, we think it is possible to identify a most-likely location of the aircraft, with unprecedented precision and certainty. This location is 35.6°S, 92.8°E. Other nearby (within about 50km essentially parallel to the 7th arc) locations east of the 7th arc are also certainly possible, as are (with lower likelihood) a range of locations on the western side of the 7th arc, near 34.7°S 92.6°E and 35.3°S 91.8°E. While we cannot be totally sure which of these locations in the southern half of the 2016-proposed search area is most likely, we do have a high degree of confidence that an impact in the southern half of the 2016-proposed search area, near 35°S, is more consistent with detection of debris in the images than is an impact in the northern half.

1 Introduction

This is our 3rd report describing oceanographic drift modelling work done in aid of the search for 9M-MRO (the Boeing 777 aircraft flying Malaysia Airlines service MH370 on 8 March 2014).

Our first report (Griffin et al., 2016) identified the 36-32°S segment of the 7th arc (especially the region near 35°S) as being the most likely site of the impact, based on where and when debris was seen and not seen on African and Australian shores (Fig 1.1), and during the initial 40-day aerial search (Fig 1.2). This work was a contribution to the First Principles Review ATSB (2016).

The 2nd report (Griffin et al., 2017) documented additional research recommended by the First Principles Review using a real Boeing 777 flaperon, rather than a replica. We measured its drift characteristics after modifying it to match the damaged one retrieved from Ile de la Reunion. This work did not change our estimate of the most likely location of the impact – it just increased confidence in the modelling by explaining more easily the 29 July 2015 Ile de la Reunion flaperon discovery.

In this third report we discuss the implications, in terms of locating 9M-MRO, of analyses by Minchin et al. (2017) of some ultra-high resolution (meter-scale) optical images acquired in March 2014.

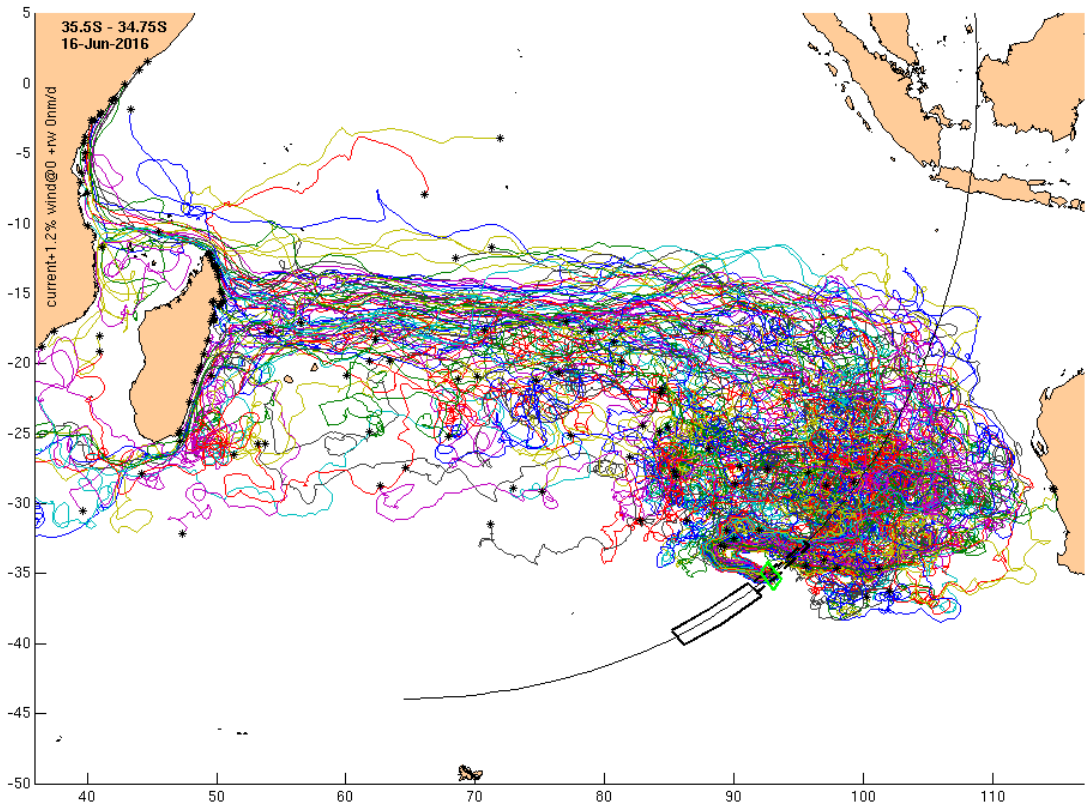

Fig. 1.1. From our first report: Trajectories from 8 March 2014 until 16 June 2016 of items starting from a narrow band of locations (the green polygon) near 35°S on the 7th arc. Trajectories from other bands of starting locations, for various durations, are available in the [on-line Appendix].

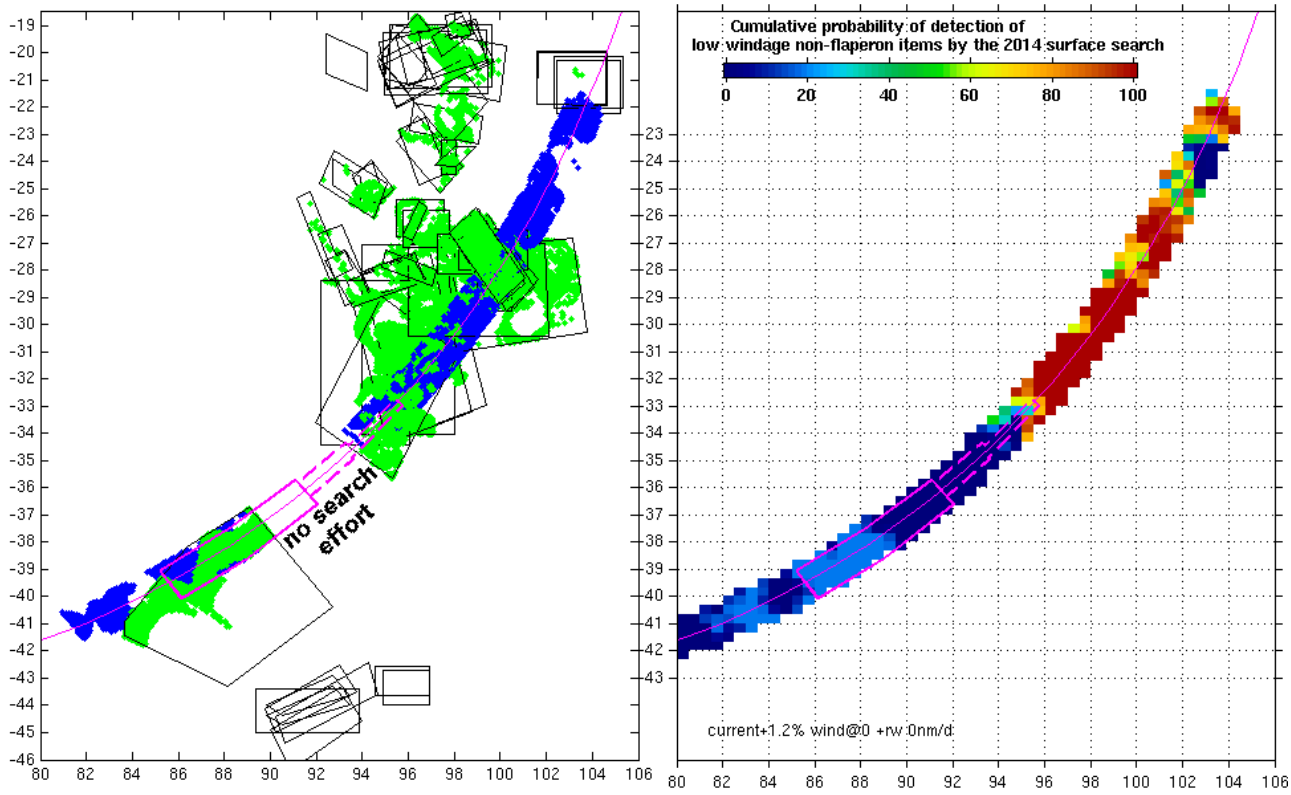

Fig. 1.2. Interpreting the surface search. The left panel shows the daily search areas as black polygons. Green zones are where low-windage debris would have drifted, having entered the water on 8 March 2014 at the locations shown in blue. The cumulative probability of detection (right panel) of potential debris shows that the aerial search effectively ruled out crash sites north of 33°S but ineffectively searched latitudes south of 34°S. The equivalent analysis for [high-windage] items is very similar.

Fig. 1.3 Genuine (left) and replica (right) flaperons at sea in calm weather during field measurements of their rate of drift *through* the water. Water movement was monitored using GPS-equipped buoys.

2 Information sources and their validity

2.1 Pleiades imagery

Minchin et al. 2017 have analysed four 0.5m-resolution Airbus Pleiades 1A visible-channel images each 25x20km, 100km apart and captured at ~4Z (midday Perth time) on 23 March 2014. These images (referred to here as PHR1-4) show 70 objects of interest, ranging from 2m to 12m in size that were sorted into 5 categories: “probably natural”, “possible natural”, “uncertain”, “possible man-made” and “probably man-made”. Minchin et al. (2017) found the greatest number (9) of probably man-made objects in image PHR4 near 34.5°S, 91.3°E, but all 4 of the images contained some of the 28 “possibly man-made” objects. These images are all within 150km of the 7th arc (to the west), between latitudes 34.5°S and 35.3°S. This is to the west of the southern half of the new search area recommended by the First Principles Review and proposed by ATSB in December 2016.

It may never be possible to know how many, if any, of these objects originated from the accident aircraft, 9M-MRO. And if they were from the aircraft, we must also remember that the bulk of the other objects may not have been very close to the locations of the images. In the absence of any explanation of what these items are, we will postulate that at least some of them are pieces of 9M-MRO, and try to determine where they were on 8 March 2014, as a way of potentially refining our estimate of the location of the crash site.

2.2 NOAA AVHRR Sea Surface Temperature imagery

If skies are clear, animation of Sea Surface Temperature (SST) imagery can reveal details of ocean circulation, significantly augmenting what can be deduced from other oceanographic techniques, including the models discussed in this and our earlier reports.

The skies in the region of present interest were only clear for a small portion of the time, but resulting views of the ocean are still quite informative. The SST imagery shown below is the result of a time-mosaic technique that is optimised for producing animations (rather than still images) to depict motion. To produce the frames of the animation, the available SST data is stepped through in 12h intervals. Gaps due to cloud are filled by the last available image of the ocean, without any temporal or spatial interpolation. This preserves the detailed information contained in good images. When viewed as an animation, the smoothly moving turbulent flow of the ocean can be seen in cloud-free regions. In cloudier areas, a patchy mosaic is created of little value. Many viewings are required to accustom the eye to the complexity of the animation – look for the times and places where motion is visible.

2.3 Satellite altimeters and eddy-resolving ocean surface currents

Our drift modelling uses the output of our Bluelink ReANalysis (BRAN) numerical model of the ocean, along with output from the ECMWF ERA-Interim numerical model of the atmosphere, to

simulate the drift of items floating on the surface of the ocean. The ocean and atmosphere models are informed by several types of satellite data as well as other point sources of information in order to be as accurate as possible. Our first report included an assessment using GDP surface drifters of the ocean model's accuracy for long-term drift. Here, we will focus on its accuracy for shorter-term drifts, using both the 2015 and 2016 versions of BRAN.

The density of satellite observations is uneven in space and time, as is, unrelatedly, the evolution of energetic features in the ocean and the atmosphere. The consequence of this is that some features of the circulation will be more accurately described by the model than others. Our earlier reports included some limited discussion of the global statistics of model error. Here, we briefly discuss the available observations that can be used to assess the accuracy of our ocean model in the vicinity of the Pleiades images, for the 15-day period between the impact of the aircraft and the capture of the images.

Satellite altimeters measure the changing topography of the sea surface. These sea-level anomaly (SLA) data are as valuable to an oceanographer as maps of atmospheric pressure are to a meteorologist. The physics is similar but the time- and space scales are different. Atmospheric pressure anomalies are much larger and faster-moving than sea-level anomalies. Figure 3.3.1 of our first report showed the satellite SLA data overlain on the resulting model SLA for 20 March 2014 for a region spanning the 41°S to 28°S segment of the 7th arc. The most notable mesoscale feature is the ridge of slightly higher (≈10cm) sea-level cutting across the 7th arc at 36°S. This ridge was observed by several satellites on several overpasses so we consider its existence (at ~50km resolution) to be quite certain, especially for the days before and after 20 March when the density of observations reached a maximum as a number of ESA Cryosat-2 overflights occurred. The density of altimeter data was less for days closer to 8 March (Fig 2.3.1), when only the CNES/NASA Jason-2 mission measured the ridge location near 91-93°E, but those data are also consistent with the flow being directed generally northwest-ward on the northern flanks of the ridge and southeast-ward on the southern side.

As mentioned in our first report, the trajectories of the Global Drifter Program drifters are in good agreement with the model estimates of the surface current. Unfortunately, none happened to be closer than 400km to the region of present interest.

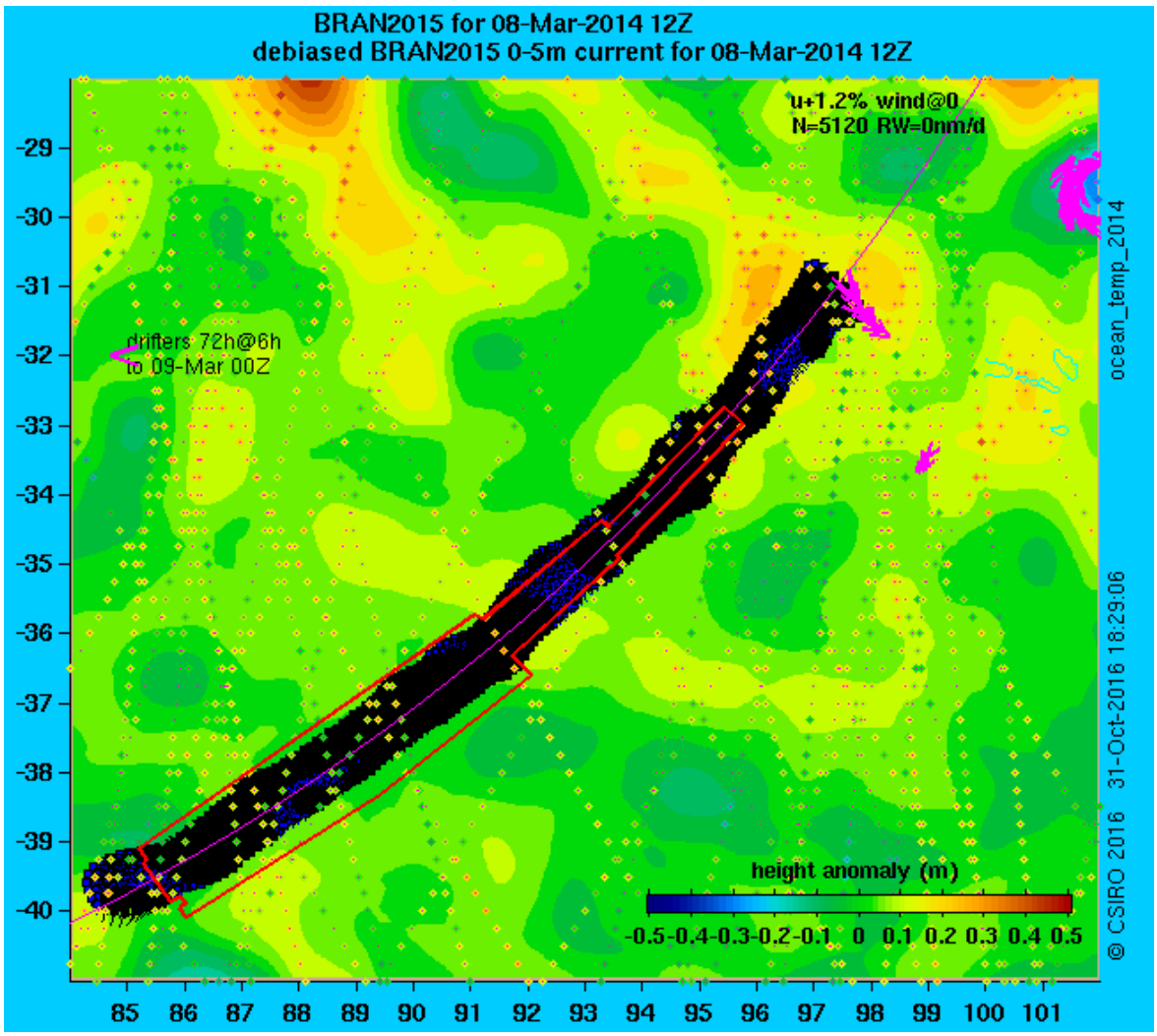

Figure 2.3.1 Model estimate of sea-level anomaly on 8 March 2014, along with the satellite altimeter measurements of sea-level anomaly that were provided to the model (shown as coloured diamonds with dark central dots, from overflights within 5 days of 8 March). The trajectories of four GDP drifters that happened to be in the region are shown as magenta arrow heads. They all travelled with positive sea-level on their left, as expected, providing independent confirmation of the model. The sea-floor area searched to date is outlined in red. For other image dates, see the [Online Appendix].

2.4 Comparison of the ocean model with SST imagery

The most cloud-free SST image for the 8-24 March interval is for 0320Z 11 March 2014 (Fig. 2.4.1). The complexity of the fronts and eddies is readily apparent. Watching the animation reveals general agreement (at the times and places of good quality imagery) of the modelled flow velocities with the motion of water bodies of different temperature, including NW-ward displacement of colder water along the diagonal of the scene. We thus have no basis to suspect that the model is any less accurate in this region for this period than it is at other times and places where we have better data for model validation.

Quantitative model velocity assessment exercises using in-situ data tend to show that comparing point measurements from the field with the 10km x 11km, daily averages from the model gives ‘error’ estimates with r.m.s. values comparable to the r.m.s. values of both the model or the observations. The model thus has skill, but cannot reproduce the small-scale features of the ocean

circulation evident in Fig. 2.4.1. Much of the velocity noise is of little consequence for trajectories, but sharp fronts and areas of bifurcating flows can lead to large errors when attempting to simulate trajectories of individual items. Thus, there are mechanisms for attenuation as well as amplification of model errors as simulated trajectories get longer and longer. Inadequate representation of small-scale features means that the model under-represents one of the most important dispersive processes, while inadequate representation of convergent fronts means that the model under-represents the anti-dispersive processes that result in 'tide lines' or 'slicks' that are commonly seen on the surface of the ocean. Where indicated below, we have adopted the common expedient of adding 'random walks' to the daily displacement of items, with r.m.s values of 5NM/day, which equates to unresolved velocities with r.m.s. amplitude of 10cm/s.

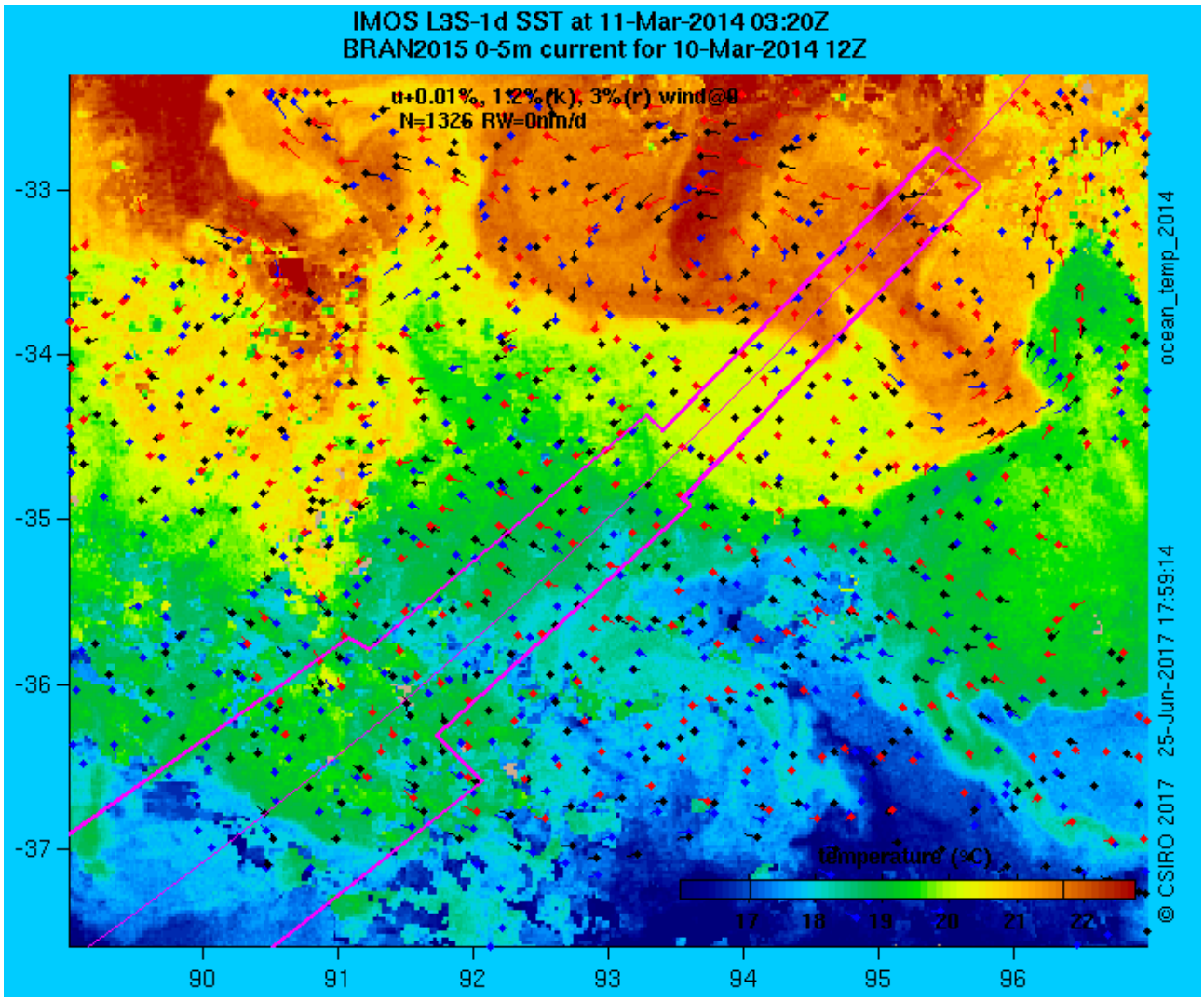

Figure 2.4.1 Time-mosaic Sea Surface Temperature image for 0320Z 11 March 2014 (or earlier – see text), with 12h-long tracks of three sorts of debris items initially distributed evenly across the panel. The blue dots move at the velocity of the BRAN2015 model's surface layer, which spans 0-5m. Large debris items hanging this deep would move at this velocity. Black dots have 1.2% of the wind velocity added, so they represent items floating flat at the surface where they are subject to Stokes Drift but not direct wind forcing. Red dots have 3% of the wind velocity added, so they represent items floating higher in the water, with exposure to the wind. Online: [animation] and [same, but using the BRAN2016 model].

3 If the Pleiades images include 9M-MRO debris, where did impact occur?

3.1 Investigative approach

We now know that 9M-MRO is not within the area searched by SONAR (ATSB 2016). This area is outlined in Figure 2.4.1 (and others) for reference. If impact was between 36°S and 32°S, as concluded by the First Principles Review, the aircraft must (obviously) be farther from the 7th arc than the region that has been searched, but still within a distance that it could have glided after commencement of descent. This is how the boundary of the new search area proposed by ATSB in Dec 2016 was defined.

Our confidence in our ability to associate the locations of the Pleiades images with points within the proposed search area is not high enough to attempt to comment on the optimal width of the two narrow (10-30km) strips east and west of the completed search area. We are quite sure, however, that we can (at least) rank the four quarters of the proposed search area in terms of likelihood of connection with the Pleiades images. We will refer here to these 4 quarters as west1 (southern half of western strip), west2 (northern half), east1 and east2 (Figure 3.1.1).

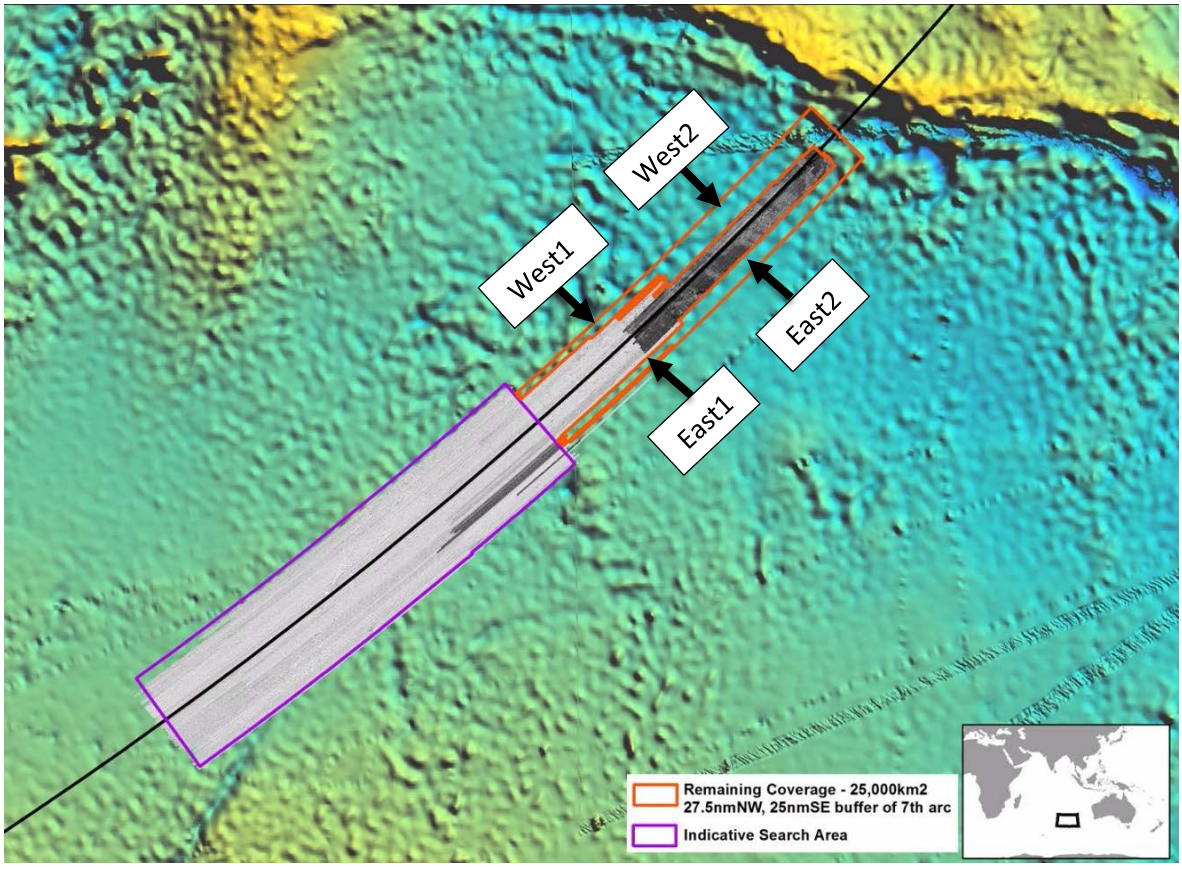

Figure 3.1.1 Bathymetric map showing (in white or black) the areas of sea-floor that have been searched and (in orange) the outline of the new proposed search area identified by the First Principles Review. Four quarters of the proposed search area are referred to in this report as west1, west2, east1 and east2. (Image provided by ATSB).

We have assessed these rankings using two ocean models, to avoid the possible pitfall of trusting either model too much. Neither of the 2015 or 2016 versions of the BRAN model have been documented in detail but we know they are fairly equally accurate (and both significant improvements on the earlier versions described by Oke et al. 2013a, b). BRAN2016 fits the assimilated SLA data more closely than BRAN2015 (compare Figure 3.2.1 with its BRAN2016 counterpart, both of which include the satellite SLA data as well as the model SLA) but this does not guarantee that the surface velocity estimates are more accurate. For the present purposes, the two models are not very different from each other, so we will discard any finding that is not equally supported by both models.

Since it is unknown whether the debris items are floating high or low in the water, we have allowed for most possibilities by computing trajectories of items with windage factors of 0, 1.2% and 3%, representing deep-drafted items, items floating flat at the sea surface, and items with substantial exposure to the wind.

3.2 Likelihood of impact in west2

The centre of PHR4 (the Pleiades image with the most “probably man-made” objects) is 290km SW of the centre of west2, for example, so the 15-day average drift velocity would have to be 290km/15d=22cm/s to the SW in order to associate items seen in PHR4 with an impact in the centre of west2. 22cm/s is a perfectly plausible mean drift speed, but a drift direction to the SW can be quite confidently ruled out at this location at this time by two independent types of Earth observation satellite data. The SST images (Fig. 3.2.1) clearly show a body of very warm water NW of west2. Anticlockwise surface velocities around the centre of this body of water can also be seen at times using the animation. This is the expected sense of rotation of warm-core eddies in the southern hemisphere. The SLA data (Fig. 3.2.1) show the high sea-level normally associated with warm-core eddies, as well as a sea-level trough cutting across the 7th arc at about 34.5°S. The associated geostrophic flow along the contours of equal sea-level (eastward near 34°S on the 7th arc) is very much in accord with what is seen in the SST imagery (surface flows are often generally along temperature fronts, with warm water on the left).

The models depend principally on the SLA data for their estimates of the surface flow velocity. These estimates differ on a point-for-point basis but the general sense of the flow is much the same and, as described above, the simulated tracks of hypothetical debris items originating from the line of points in west2 rotate in an anticlockwise direction. The three types of debris, being progressively more affected by the wind, move only slightly differently, showing that the effect of the wind is secondary here to the effect of the current.

In summary, both the BRAN2015 and BRAN2016 models suggest that impact sites in west2 are too far north-east to be associated with any type of debris (high, low or no windage) potentially identified in all the images.

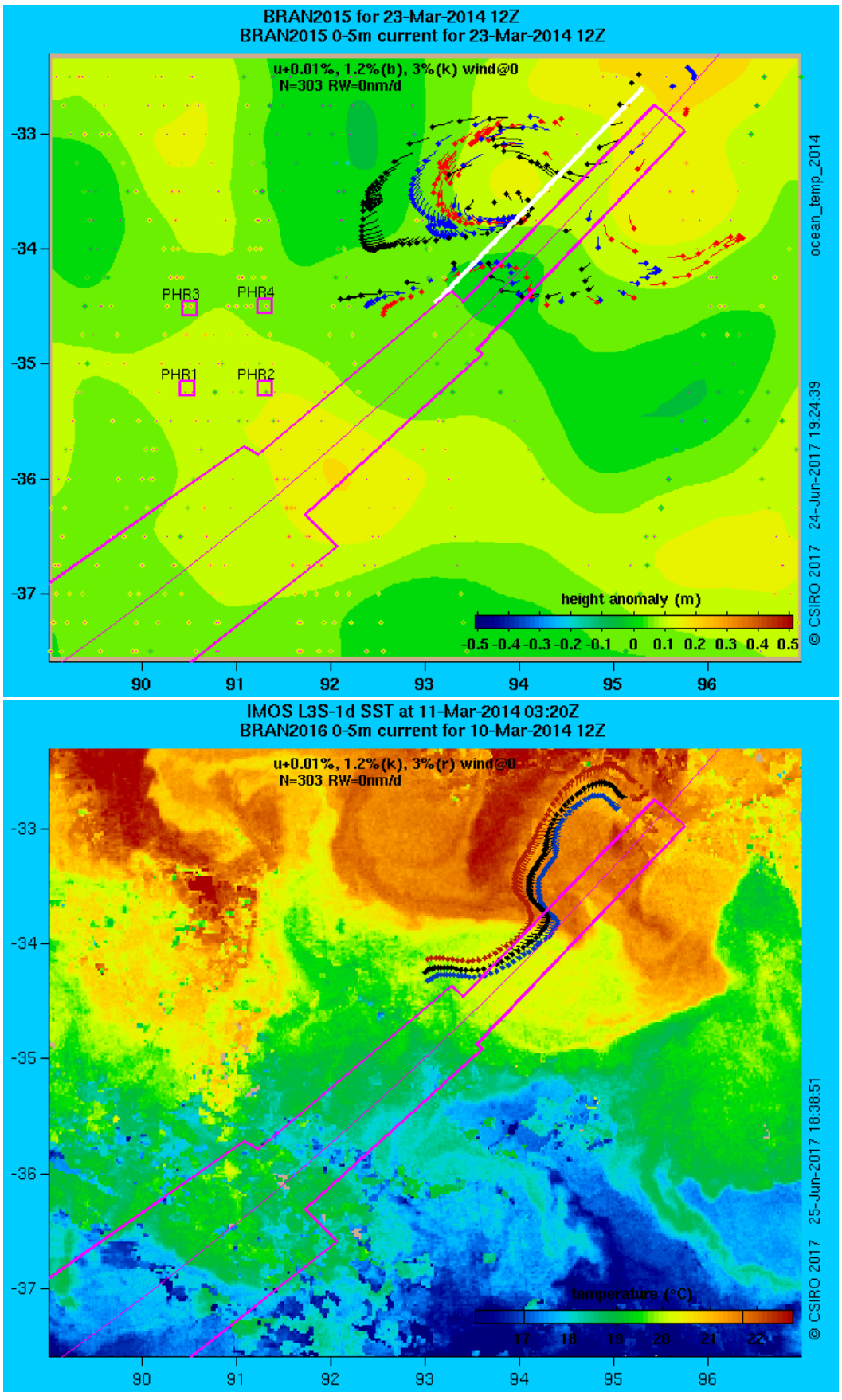

Figure 3.2.1 Simulated drift of three types of hypothetical debris items distributed along a line (shown) in west2 on 8 March 2014. Upper: 23 March positions overlain on sea-level. Lower: 11 March overlain on satellite SST. Sequences: BRAN2015 [SLA] [SST], BRAN2016 [SLA] [SST].

3.3 Likelihood of impact in east2

The east2 region is even farther away from the images than the west2 region, but still within the same flow regime, so the comments above are also very relevant here. The conclusion is the same.

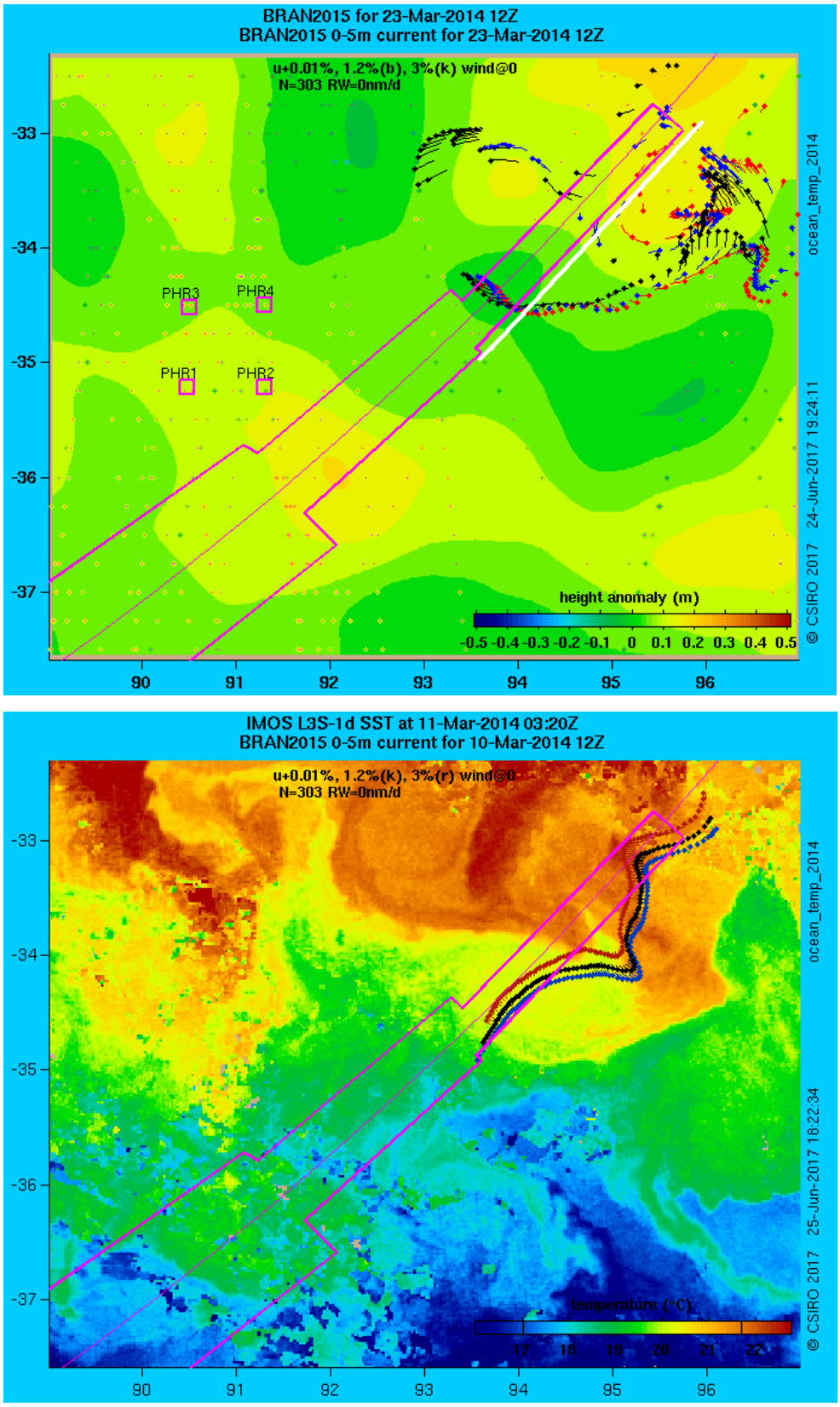

Figure 3.3.1 As above, but for east2. Sequences: BRAN2015 [SLA] [SST], BRAN2016 [SLA] [SST].

3.4 Likelihood of impact in west 1 or east 1

Results are very different for west1 (Figure 3.4.1), which is the closest zone to the images (100km to PHR4) and east1 (Figure 3.4.2) which is 200km from PHR4. The dispersal (stretching, rotation and displacement) of the lines of hypothetical debris items is much less for west1 and east1 than shown above for west2 and east2, where the flow speeds were higher and more complex. The strongest flow is near the midpoints of the lines, northwest-ward (generally towards the locations of the images) along the contours of equal sea-level (with the sea-level ridge on the left and the trough on the right), cutting across the 7th arc at 35.3°S. The speed of this flow according to the models is about 20cm/s (Fig. 3.4.3), which is too fast to associate many of the west1 points with PHR4, for example, but about right for the points in east1 near the core of the flow.

For Figure 3.4.3 we have included a representation of unresolved turbulence using random walks (discussed above) and computed trajectories of items from just a single location – 35.6°S, 92.8°E within east1. This shows that according to both models, there is a single location (within east1) which can very plausibly be linked to the potential appearance of all three types of debris in PHR4 (which had the greatest number of probably man-made objects).

Other nearby (within about 50km essentially parallel to the 7th arc) locations within east1 are also very plausibly linked with the imagery, as are a range of locations in west1, especially near 34.7°S 92.6°E and 35.3°S 91.8°E (Fig. 3.4.4). These locations in west1 are on either side of the core of the strong flow cutting across the 7th arc, where the flow speed is lower. The two models disagree over which of the two locations is more likely, as can be seen by scrutinizing the details of the modelled trajectories using Google Earth (Fig. 3.4.5).

To confidently discriminate the likelihood of these three nominated locations of the missing aircraft is possibly beyond the capabilities of the models we have used here, simply because they do not have fine-enough spatial resolution with which to represent the details of the ocean circulation. Finer models do exist and could be used for this task but, while this might obviate the need to represent the mixing effects of finer-scale using random numbers, they are not guaranteed to be substantially more accurate in terms of net drift, for lack of observations to constrain the models to match the real world.

The 100km spacing of the Pleiades images to which we have access is another fundamental limitation, as is, of course, the uncertainty over which objects within the images are indeed pieces of 9M-MRO.

In the meantime, however, we consider the location in east1 to be the more likely because it is the only one indicated by both models.

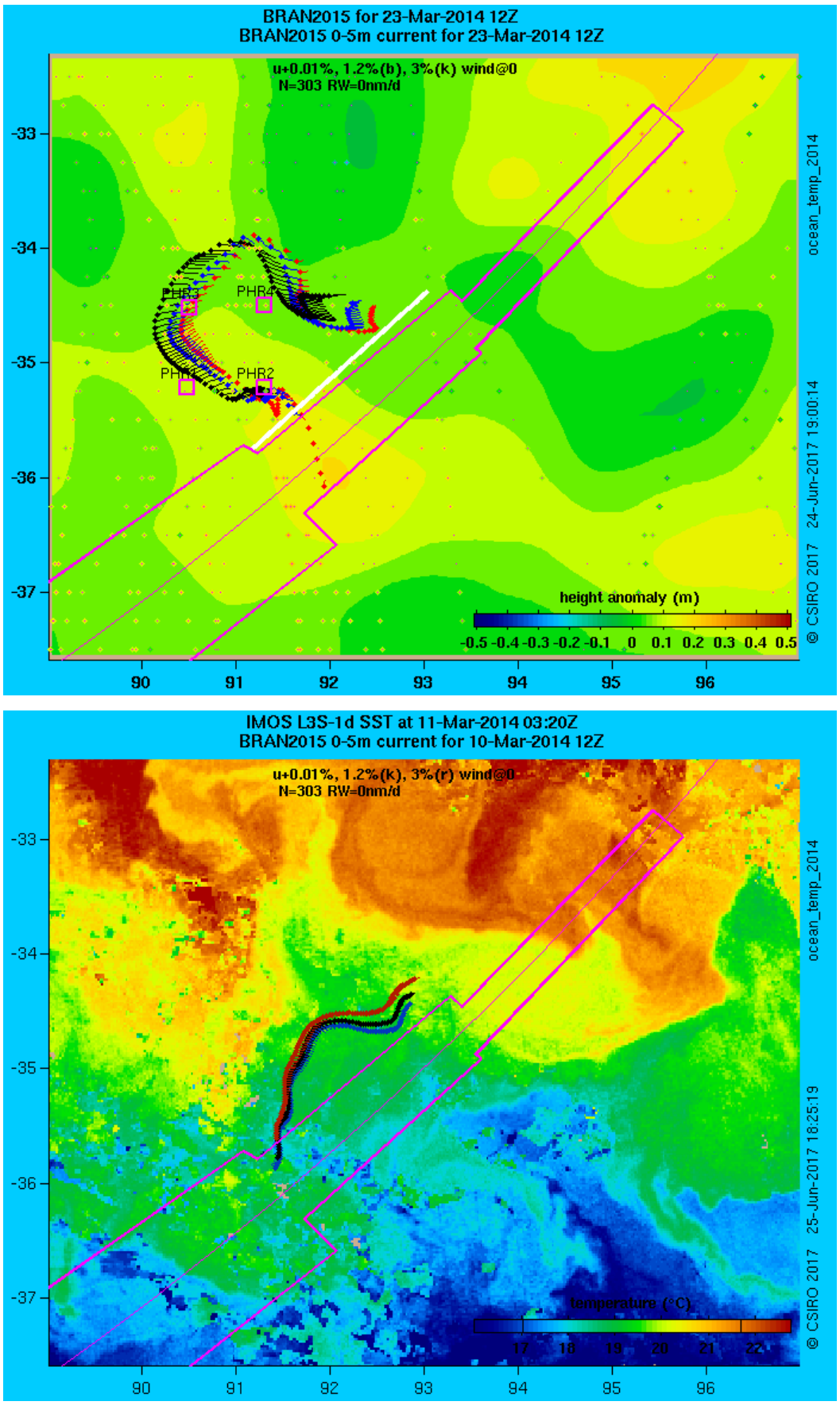

Figure 3.4.1 As above, but for west1. Sequences: BRAN2015 [SLA] [SST], BRAN2016 [SLA] [SST].

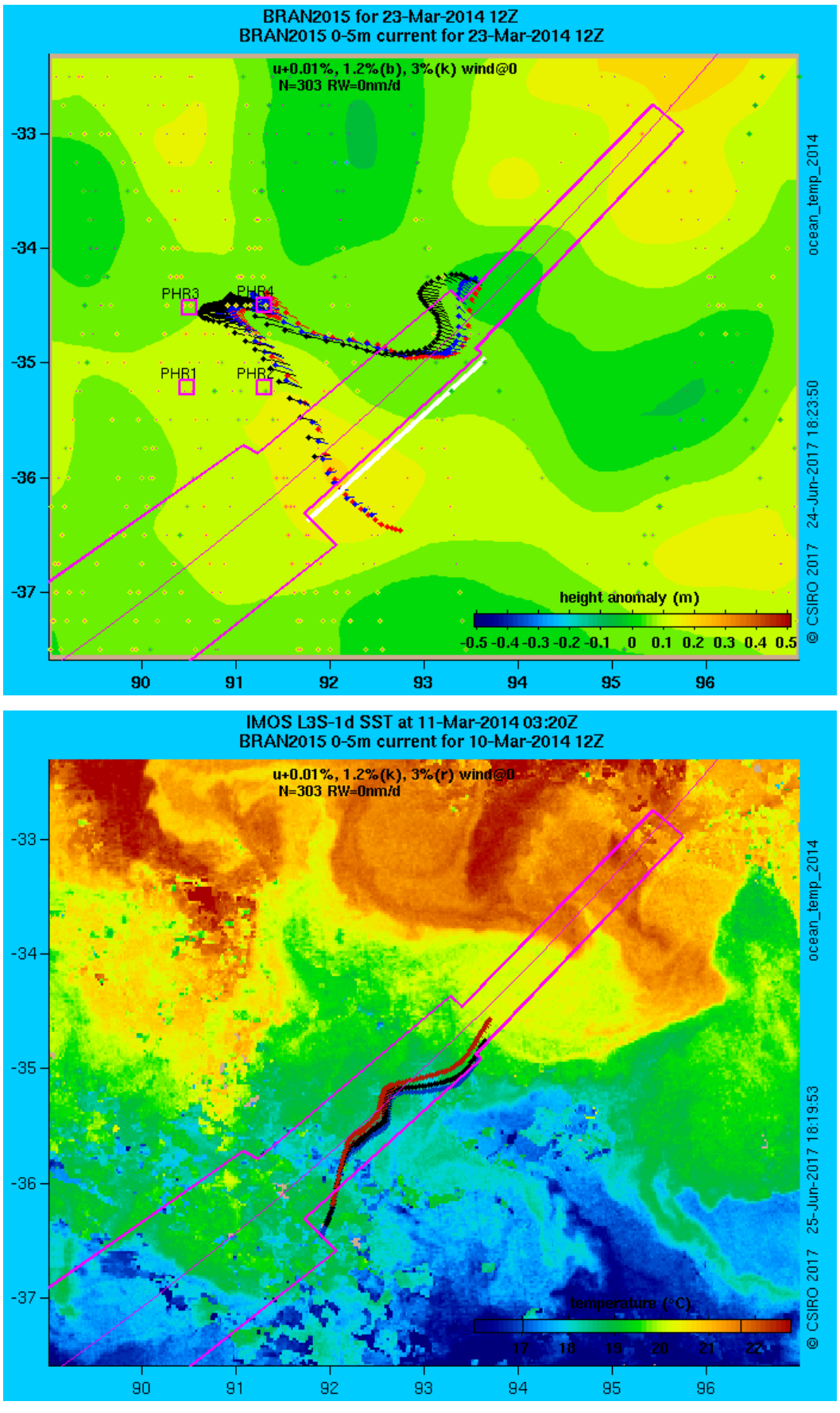

Figure 3.4.2 As above, but for east1. Sequences: BRAN2015 [SLA] [SST], BRAN2016 [SLA] [SST].

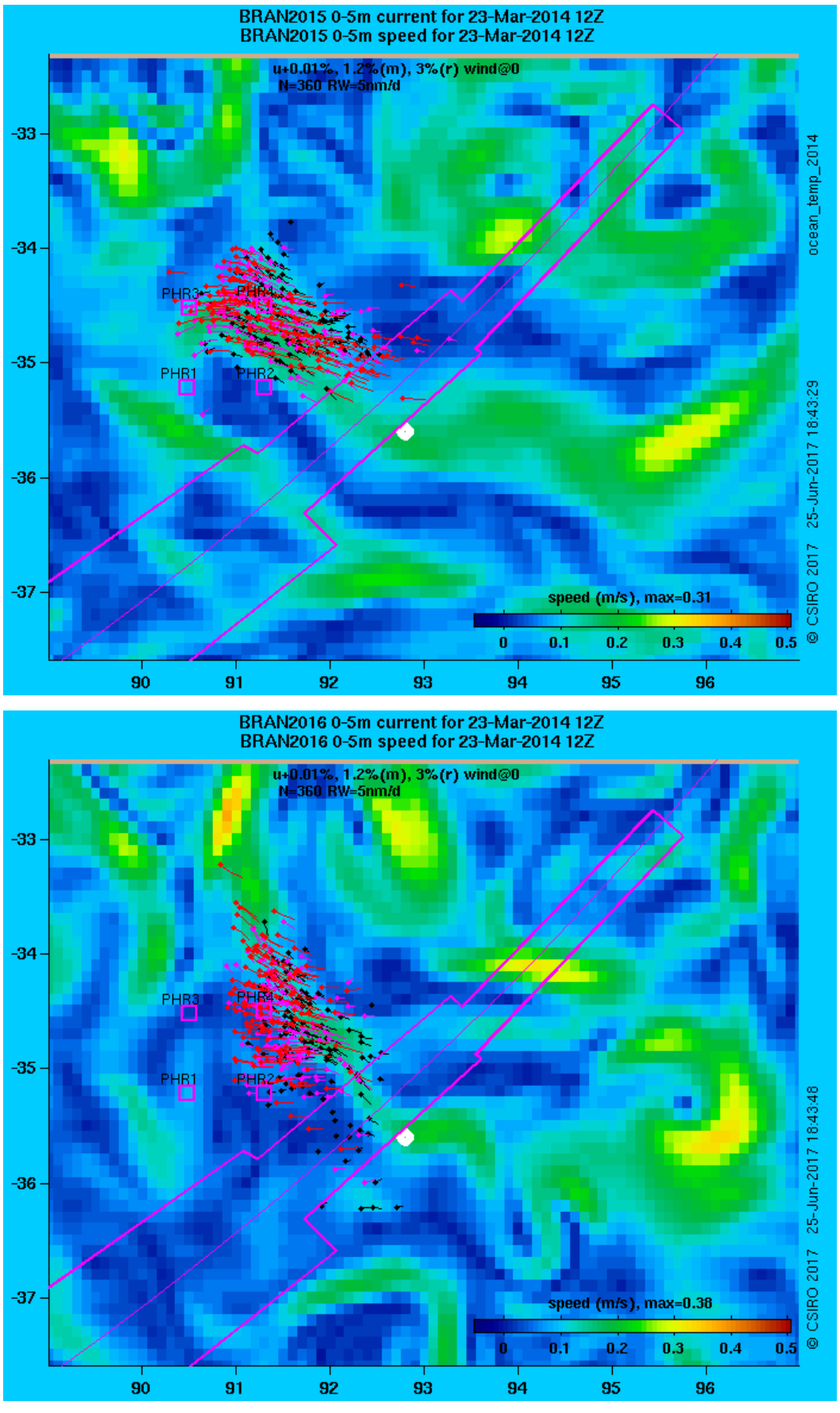

Figure 3.4.3 As above, but for a single impact location (35.6°S, 92.8°E), unresolved turbulence represented by 5NM/d random walks, and colour-fill showing speed instead of sea-level anomaly. Upper: using BRAN2015 [image sequence], lower: using BRAN2016 [image sequence].

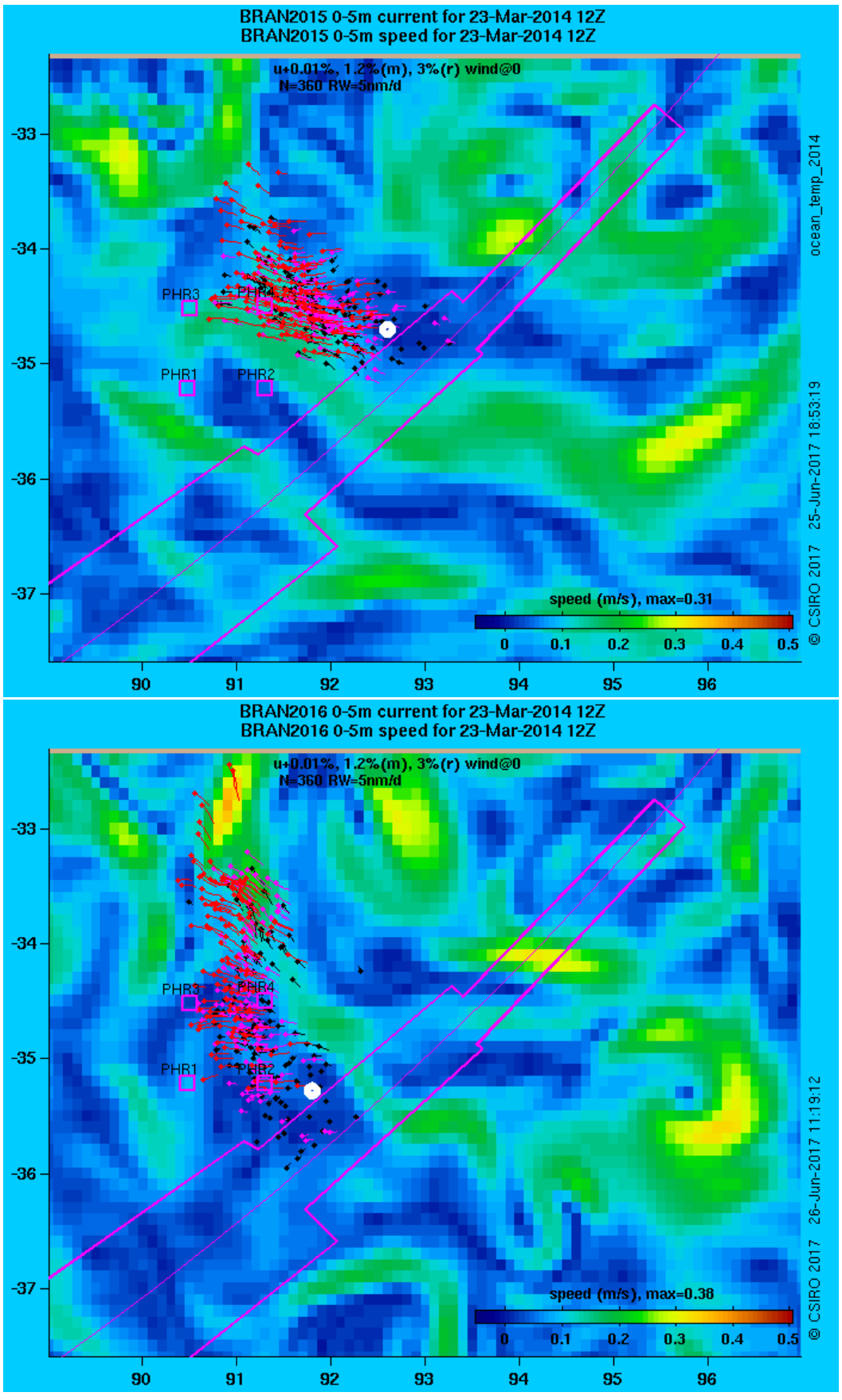

Figure 3.4.4 As above, but for impact locations at 34.7°S, 92.6°E (upper) and 35.3°S, 91.8°E (lower), using [BRAN2015] and [BRAN2016], respectively.

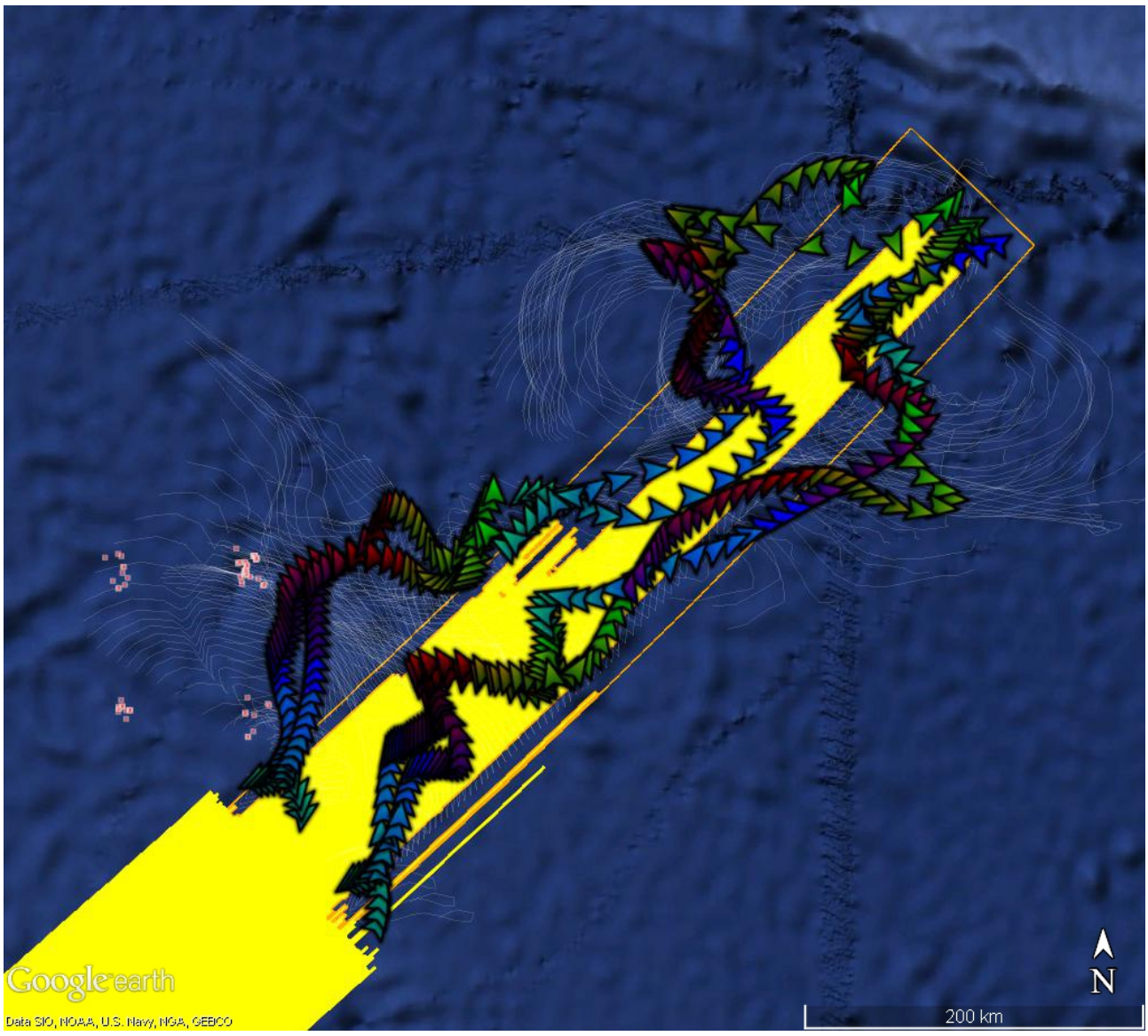

Figure 3.4.5 Google Earth screenshot showing locations on 13 March 2014 of hypothetical debris items (with 1.2% windage) originating in the east1&2 and west1&2 regions as estimated by BRAN2015 and BRAN2016. Locations of all objects of interest in the 23 March 2014 Pleiades images are also shown, as is the outline of the new search area proposed in December 2016 and the area searched up to that time. [Kmz files of the modelled trajectories]

3.5 Could the debris field have spanned 150km after 15 days?

The 4 Pleiades images are about 100km apart, and may all include parts of the missing aircraft, as might adjacent un-imaged regions. The result that a single impact location could be consistent with debris sightings 15 days after impact ~150km apart is only obtained if random walks (of reasonable size) are included in the simulation. Our global, coarse-resolution models cannot otherwise explain that amount of diffusion, other than by manifestly being unable to hindcast the velocity of drifting buoys at better than 20cm/s r.m.s., thereby providing an upper bound on the amplitude of the unresolved velocities.

To achieve a separation of 150km over 15 days, two particles need to travel with an average differential velocity of 12cm/s. The magnitude of their differential velocity is less likely to be this

great at the initial time, when their distance apart is presumably less than 1km in the case of an aircraft hitting the surface of the ocean. But after a few days of slow diffusion, greater differential velocities will be encountered, stretching the cloud of debris items into the elongated spiral shapes that are routinely seen in images of the ocean. The model has velocity gradients of 30cm/s over 50km distances. In the real world, such gradients will exist over shorter distances. Thus we believe that while our model cannot deterministically simulate diffusion from a point source to a 150km cloud, we do not think this (or perhaps even a greater) amount of dispersal is large enough to challenge the proposition that many of the man-made objects potentially identified in the various images were at the same location on 8 March. If it could be independently shown that only one image (e.g. PHR4) shows pieces of 9M-MRO, this question obviously disappears.

3.6 Trajectories across the Indian Ocean

To demonstrate the degree to which the scenario of the impact occurring at 35.6°S, 92.8°E is consistent with the

1) absence of detections during the surface search,
2) absence of debris findings on the Australian coast,
3) discovery of the flaperon at Ile de la Reunion on 29 July 2015 and
4) discovery of debris on African shores from December 2015 onwards,

Figure 3.6.1 shows the simulated trajectories of debris items from this single point of origin. For this simulation we have used the BRAN2015 model, whose long-term drift bias we carefully assessed and corrected for our first report. Trajectories have been calculated for low- and high-windage items and also for the flaperon whose additional leeway speed and finite leeway angle we determined empirically. Panels show the trajectories of items (non-flaperon for all but one) from the time of impact up to 1) 2 April when the last of the nearby aerial search campaigns was finished, 2) mid November when the debris field was as close to Australia as the simulation ever placed it, 3) July 2015 when the flaperon was discovered, 4) December 2015 when ‘Roy’ was first photographed in S. Africa and 5) July 2016, by which time many items had been reported on African coasts or islands of the western Indian Ocean.

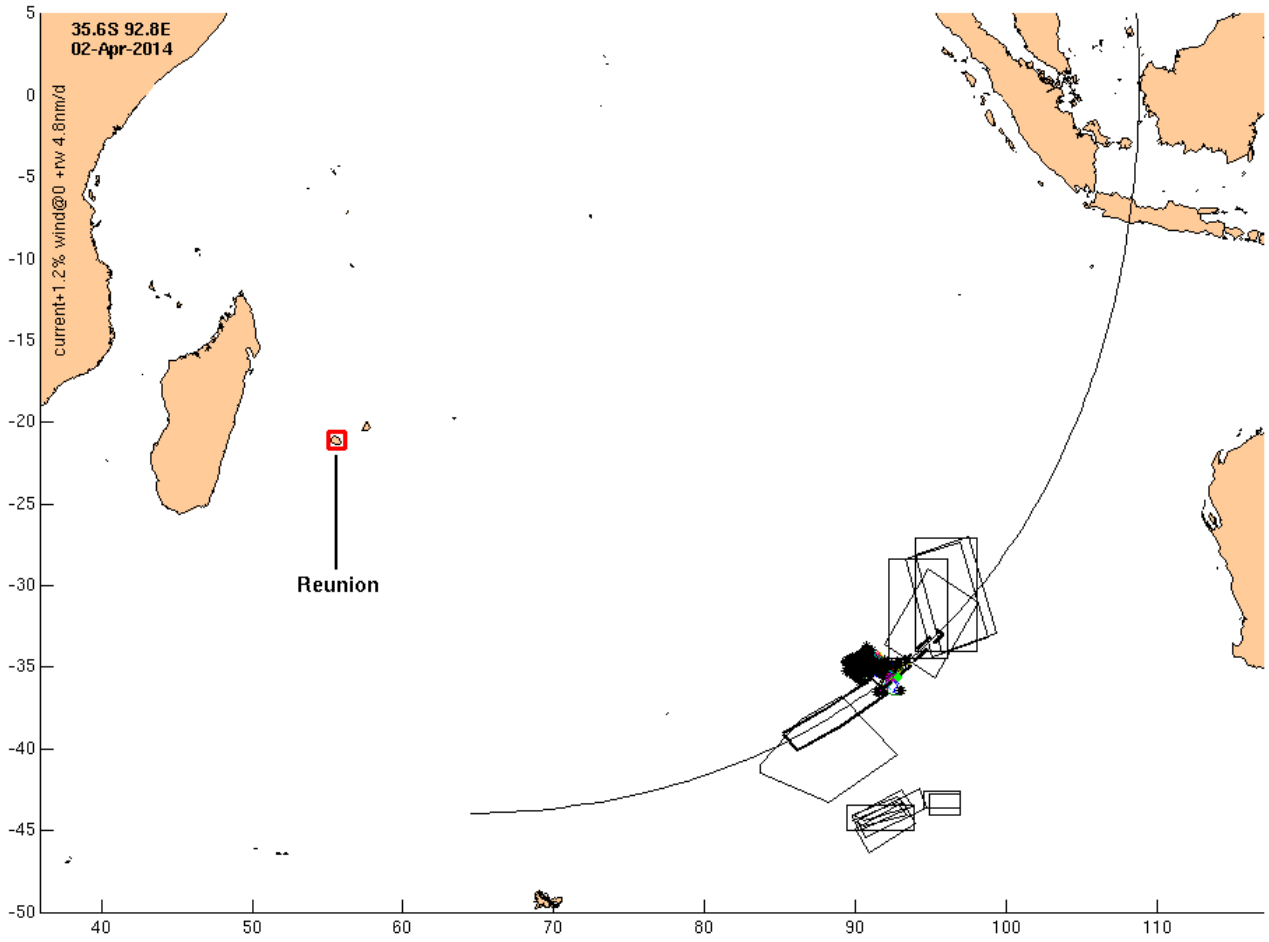
35.6S 92.8E
02-Apr-2014
current+1.2% wind@0 +rw 4.8nm/d
Reunion
5
0
-5
-10
-15
-20
-25
-30
-35
-40
-45
-50
40
50
60
70
80
90
100
110

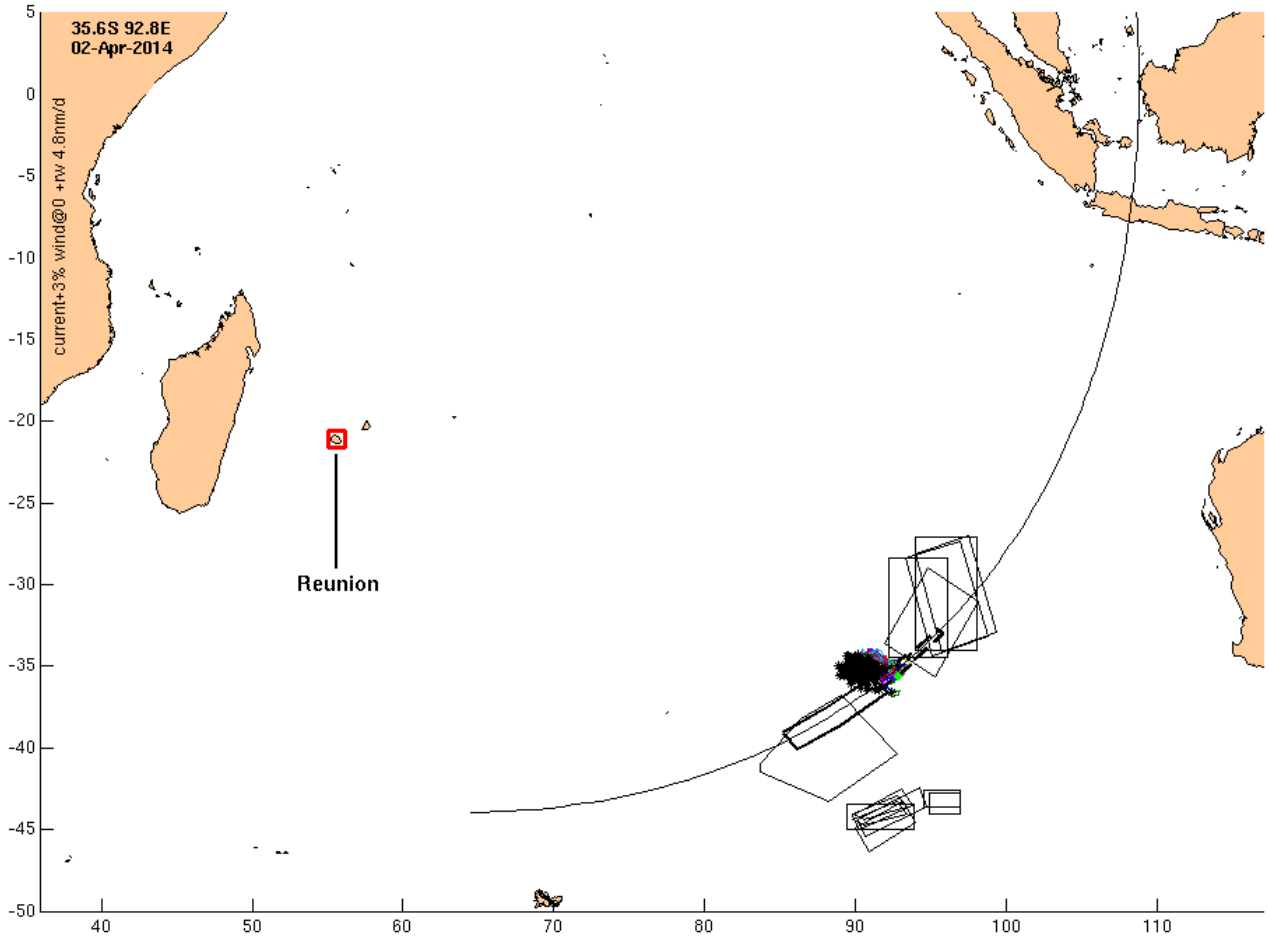
35.6S 92.8E
02-Apr-2014
current+3% wind@0 +rw 4.8nm/d
Reunion
5
0
-5
-10
-15
-20
-25
-30
-35
-40
-45
-50
40
50
60
70
80
90
100
110

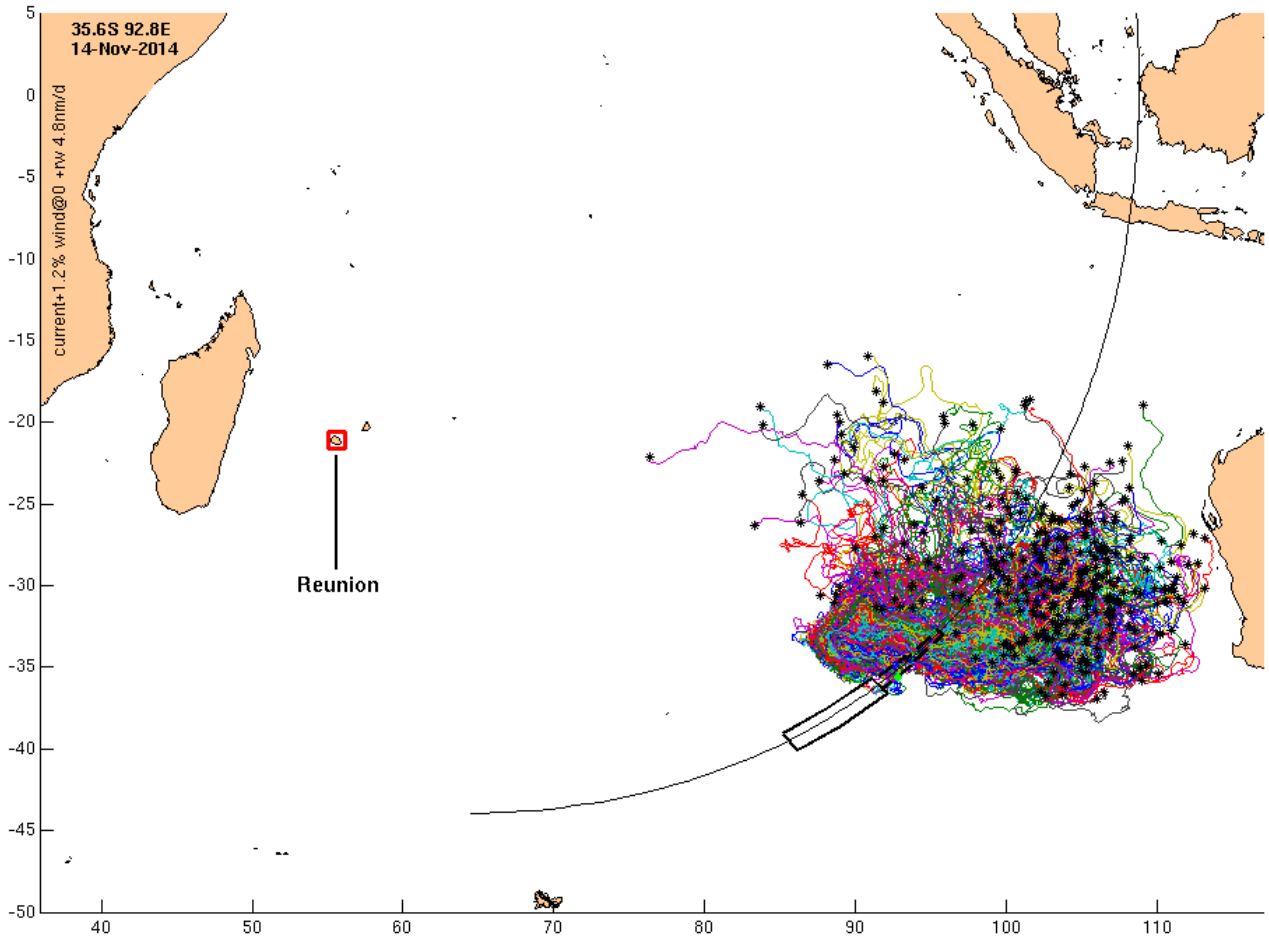
35.6S 92.8E
14-Nov-2014
current+1.2% wind@0 +rw 4.8nm/d
Reunion
5
0
-5
-10
-15
-20
-25
-30
-35
-40
-45
-50
40
50
60
70
80
90
100
110

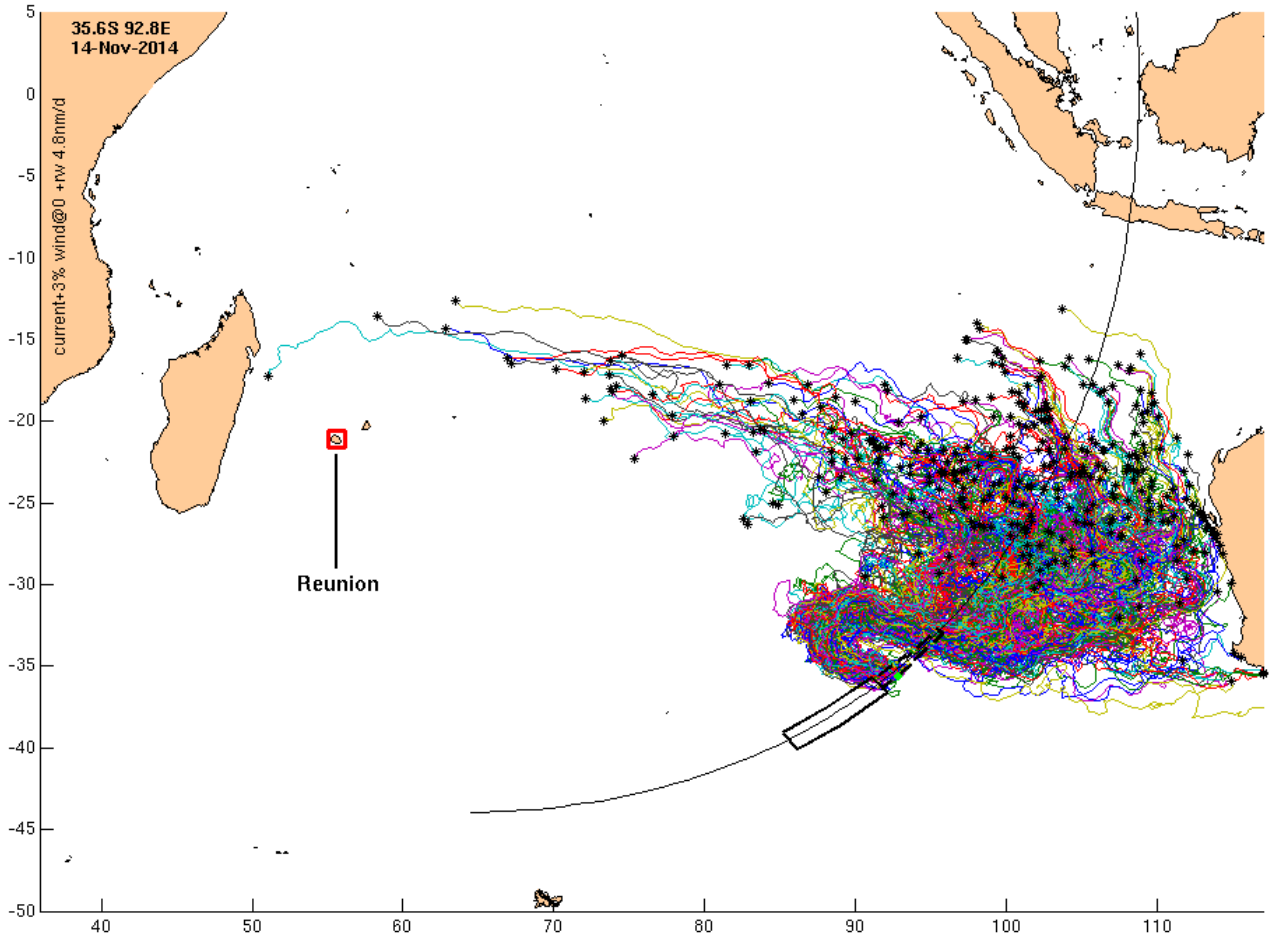
35.6S 92.8E
14-Nov-2014
current+3% wind@0 +rw 4.8nm/d
Reunion
5
0
-5
-10
-15
-20
-25
-30
-35
-40
-45
-50
40
50
60
70
80
90
100
110

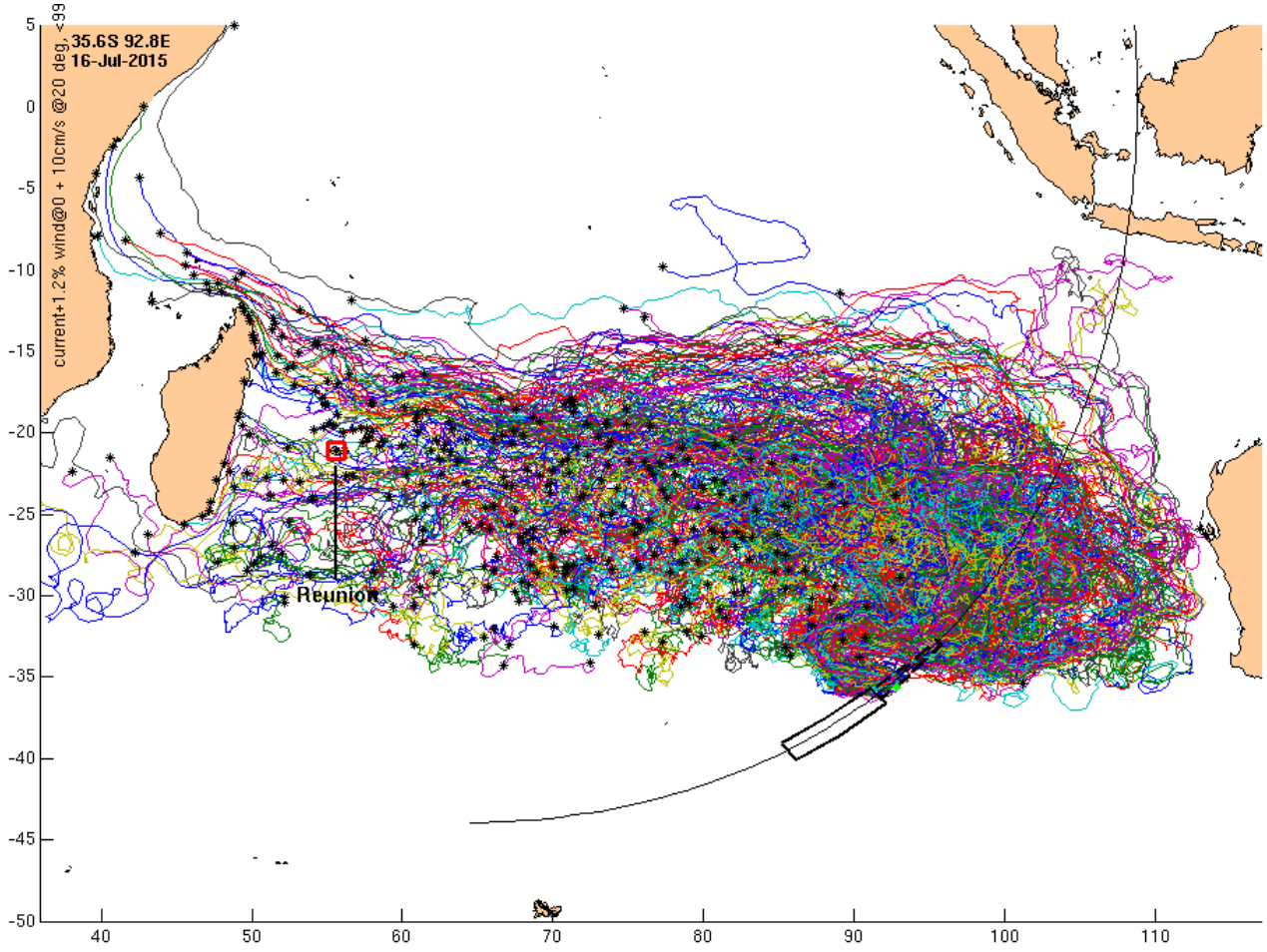
35.6S 92.8E
16-Jul-2015
current+1.2% wind@0 + 10cm/s @20 deg, <99
Reunion
5
0
-5
-10
-15
-20
-25
-30
-35
-40
-45
-50
40
50
60
70
80
90
100
110

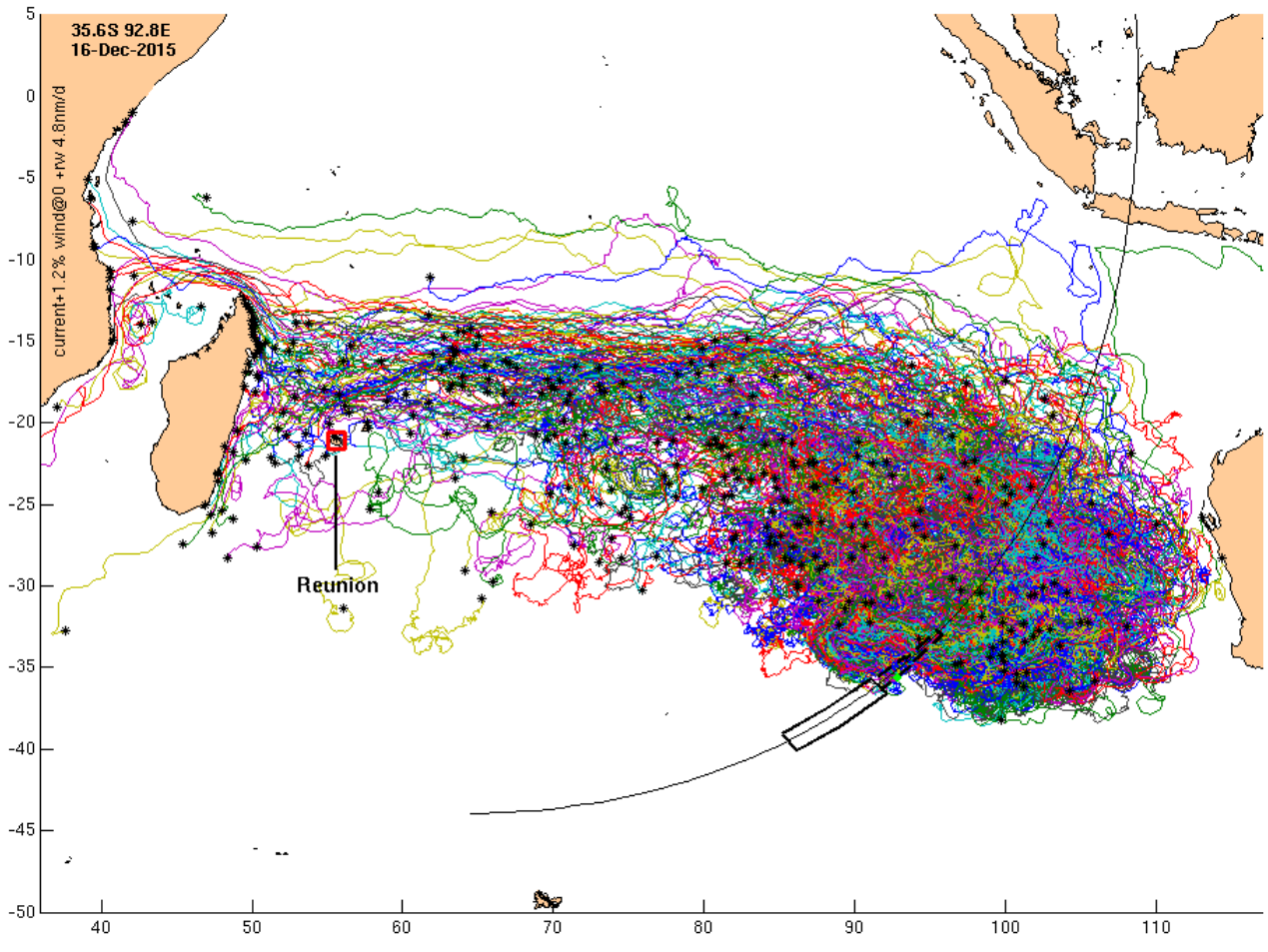
35.6S 92.8E
16-Dec-2015
current+1.2% wind@0 +rw 4.8nm/d
Reunion
5
0
-5
-10
-15
-20
-25
-30
-35
-40
-45
-50
40
50
60
70
80
90
100
110

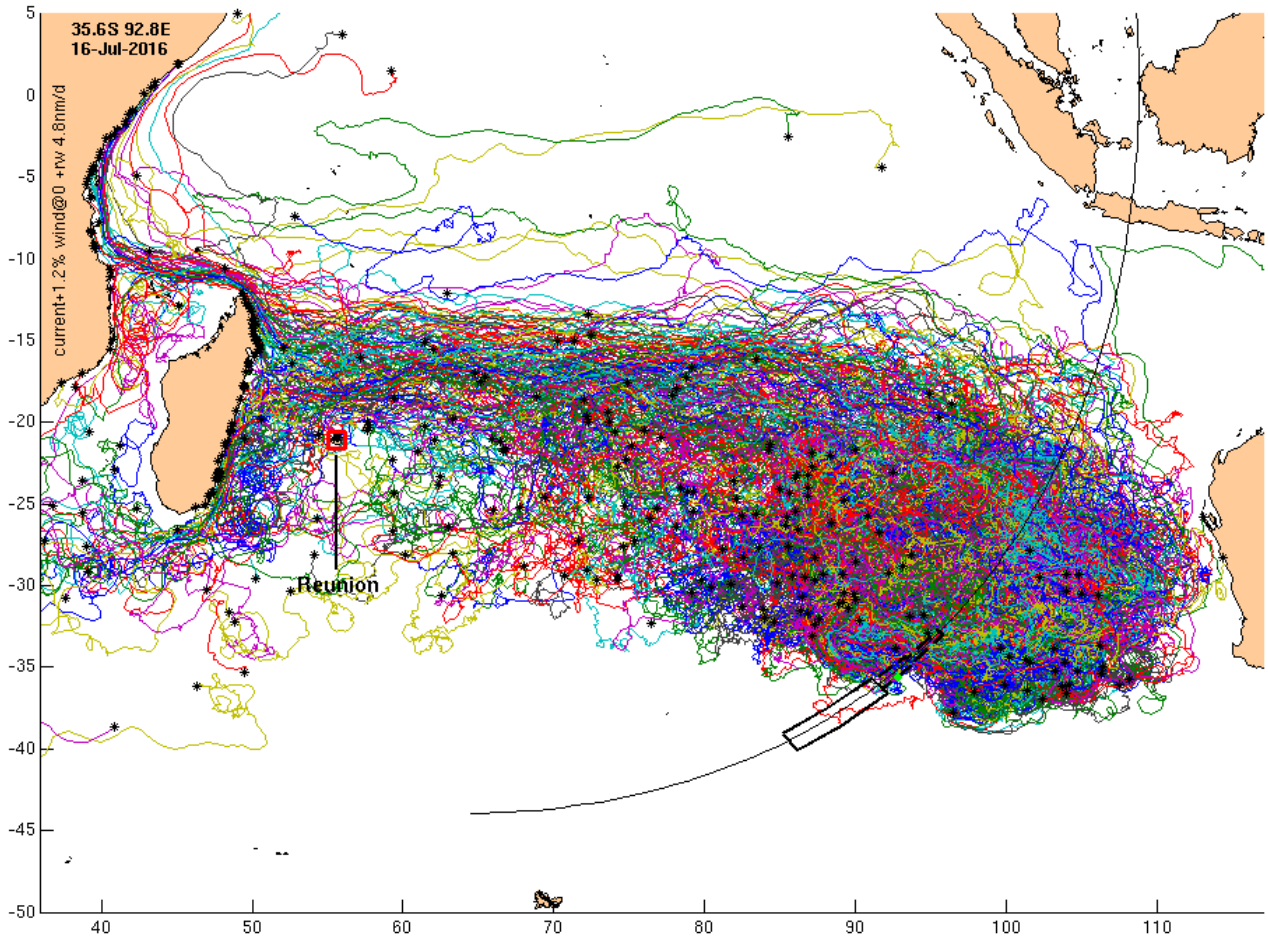

Figure 3.6.1 Trajectories (randomly coloured lines) up to, and positions (black dots) at 5 key dates (shown at top left) of [low-windage items] (panels 1, 3, 6 and 7), [high windage] items (panels 2 and 4) and the [flaperon] (panel 5 for July 2015), all of which originated at 35.6°S, 92.8°E on 8 March 2014.

Panels 1 and 2 of Figure 3.6.1 show that if the impact was indeed at 35.6°S, 92.8°E then it is not surprising that no detections were made during any of the aerial searches conducted in March 2014. Panel 3 shows that there is only a very small chance that any of the low-windage debris would have washed up on the coast of Australia. Panel 4 shows that a few items of high-windage debris – if they were still afloat – are hindcast to have washed up at some remote locations on Australian shores. Panel 5 shows that Ile de la Reunion was not far from being the flaperon's most likely position on 29 July 2015. Panel 6 does not extend as far south as Mosul Bay, where the piece of engine cowling bearing the Rolls Royce insignia was found, but the small number of items heading that way suggests that the model does not easily explain this finding. To reach this farthest away location before any other findings occurred suggests that either 1) it did travel, by chance, faster than most items, or 2) other strandings occurred in 2015 but were not reported. The model is consistent with both scenarios – it has items starting to arrive on the east coast of Madagascar as well as Tanzania in December 2015. Panel 7 shows that by July 2016, a large fraction of all the debris items have reached the western half of the Indian ocean, thus explaining the large number of finds.

4 Conclusion

Assuming that some of the objects identified in the Pleiades images are indeed debris items from 9M-MRO, we have shown that there is an impact location that is consistent with those sightings, as well as all the other evidence reviewed by the First Principles Review. This location is 35.6°S, 92.8°E. Other nearby (within about 50km essentially parallel to the 7th arc) locations east of the 7th arc are also certainly possible, as are (with lower likelihood) a range of locations on the western side of the 7th arc, near 34.7°S 92.6°E and 35.3°S 91.8°E. While we cannot be totally sure which of these locations in the southern half of the 2016-proposed search area is most likely, we do have a high degree of confidence that an impact in the southern half of the search area is more consistent with detection of debris in the Pleiades images than is an impact in the northern half.

5 Glossary

7th arc. The curved line defined by a set of points that are all equidistant from the Inmarsat satellite via which 9M-MRO was in communication with a satellite ground station. This distance is inferred from the Burst Timing Offset associated with the 7th communication since losing contact with traffic controllers. For more detail, see ATSB 2015.

9M-MRO. The designation of the particular Boeing 777 aircraft operating Malaysia Airlines Flight MH-370 on 8 March 2014.

Altimeter. An instrument carried by an earth-observation satellite that measures two quantities extremely accurately – 1) its position in space and 2) the distance to the surface of the ocean directly below – in order to estimate the departure of the sea surface from a reference surface. This project used data from the following missions operated by the respective space agencies: Jason-2 (NASA and CNES), CryoSat2 (ESA), AltiKa (CNES and ISRO). FFI see http://oceancurrent.imos.org.au/glossary.php

BRAN. Bluelink ReAnalysis – Results from a global 1/10th degree resolution (~11km at the equator) ocean general circulation model that assimilates ocean observations to constrain the modelled circulation to reality. BRAN2015 is the version of BRAN executed in the year 2015, and spanned just 7 years (2009-2016). It was our first long, data-assimilating model run with 0.1° resolution for the entire globe, as well as having other physics refinements over the 2014 version, which had coarse resolution outside the Australasian region. BRAN2016 was completed in 2016 and spanned the full extent (1994-2016) of the period for which there is data from satellite altimeters. There were no important changes to the model physics, but there was a change from using the NOAA GFDL MOM4 dynamical core to MOM5. A minor error in the output file format (inappropriate compression) of BRAN2016 explains the jagged contours of the SLA maps shown in this report.

GDP. Global Drifter Program, housed at the US National Oceanic and Atmospheric Administration Atlantic Oceanographic and Meteorological Laboratory (NOAA AOML). FFI see http://www.aoml.noaa.gov/phod/dac/gdp_information.php

NM. Nautical mile. Equivalent to one minute of latitude, or 1.85km.

SLA. Sea Level Anomaly. The departure of (non-tidal, and with the quasi-isostatic response to atmospheric pressure subtracted) sea-level from the time-mean value. FFI.

SST. Sea Surface Temperature. This is measured by the Advanced Very High Resolution Radiometer (AVHRR) sensor carried by the (US) National Oceanic and Atmospheric Administration (NOAA) Polar Operational Environmental Satellites (POES) and has been a mainstay of oceanographic research for decades. Australia receives the direct-broadcast High Resolution Picture Transmission (HRPT) data at several ground stations. A variety of AVHRR SST data products are distributed by the Bureau of Meteorology and CSIRO as part of Australia's Integrated Marine Observing System (IMOS) [FFI]. For this report, we have used the L3S-1d product available from the [IMOS SST Thredds server].

Stokes Drift. Movement in the direction of waves due to the fact that the orbital velocity of a parcel of water, due to the passage of a wave, is not a closed ellipse.

Windage. Strictly speaking, this is defined as the wind-driven motion with respect to the water of a floating object, due to the force of the wind on the object. More commonly, it is taken to be the wind-driven motion with respect to specific measure of the surface velocity. If that measure does not include the Stokes Drift or other wind-related quantities, then the windage factor (ratio of windage to wind speed) will be a measure of them too.

References

ATSB (2016) MH370 – First Principles Review Report. ATSB, 20 December 2016.

Minchin, S., Mueller, N., Lewis, A., Byrne, G., Tran, M., 2017. Summary of imagery analyses for non-natural objects in support of the search for Flight MH370: Results from the analysis of imagery from the PLEIADES 1A satellite undertaken by Geoscience Australia. Record 2017/13. Geoscience Australia, Canberra. http://dx.doi.org/10.11636/Record.2017.013

Griffin DA, Oke PR, Jones EM (2016). The search for MH370 and ocean surface drift. CSIRO Oceans and Atmosphere, Australia. Report number EP167888. 8 December 2016. DOI: 10.4225/08/5892224dec08c

Griffin DA, Oke PR, Jones EM (2017). The search for MH370 and ocean surface drift. CSIRO Oceans and Atmosphere, Australia. Report number EP172633. 13 April 2017. DOI: https://doi.org/10.4225/08/58fba83e73f2b

Oke PR, Sakov P, Cahill ML, Dunn JR, Fiedler R, Griffin DA, Mansbridge JV, Ridgway KR, Schiller A (2013a). Towards a dynamically balanced eddy-resolving ocean reanalysis: BRAN3. *Ocean Modelling* **67**, 52-70, doi: dx.doi.org/10.1016/j.ocemod.2013.03.008

Oke PR, Griffin DA, Schiller A, Matear RJ, Fiedler R, Mansbridge JV, Lenton A, Cahill M, Chamberlain MA, Ridgway K (2013b). Evaluation of a near-global eddy-resolving ocean model. *Geoscientific Model Development* **6**, 591-615, doi:10.5194/gmd-6-591-2013.